Experimental and Thermodynamic Study of Nickel-Base Alloys containing Chromium Carbides: Part I -Study of the Ni-30wt.%Cr-xC System over the [0 to 2.0%wt.C] Range

P. Berthod, P. Lemoine, L. Aranda

Experimental and Thermodynamic Study of Nickel-Base Alloys containing Chromium Carbides:
Part I - Study of the Ni-30wt.%Cr-xC System over the [0 to 2.0%wt.C] Range

P. Berthod *, P. Lemoine, L. Aranda
Laboratoire de Chimie du Solide Minéral (UMR 7555),
Faculté des Sciences et Techniques, UHP Nancy 1, Nancy - Université
BP 239, 54506 Vandoeuvre-lès-Nancy – France
* Corresponding author's e-mail : patrice.berthod@centraliens-lille.org
* Correspond. author's phone number: (33)383684666 and fax number: (33)383684611

Post-print version of the article *Calphad, Vol. 32, pp. 485-491 (2008); doi:10.1016/j.calphad.2008.06.006*

Abstract. Seven {Ni-30wt.%Cr}-based alloys containing between 0 and 2 wt.%C, were produced by casting and heat treated at 1,000, 1,100 and 1,200°C. Their solidus and liquidus temperatures and surface fractions of the existing phases were experimentally determined. These results were compared to calculations performed with Thermo-Calc in order to proof the database. Additional thermodynamic calculations were used for the exploration of microstructures for other Cr and C contents, in or out the interval of values studied above. The calculated solidus temperatures and the volume fractions of carbides are in good agreement with experiments. This allowed using calculations to explore with accuracy the microstructure variation in this ternary system: fractions of carbides for higher contents in C or other Cr contents, or conditions on C for avoiding carbides (solvus determination).

Keywords: Nickel-Chromium alloys; Chromium carbides; Experimental characterization; Thermodynamic calculations

1. Introduction

Among the nickel-based alloys for applications at high temperature (e.g. γ/γ'-type superalloys) there are other nickel alloys strengthened by carbides [1–2]. They are notably considered when chromium is more suitable than aluminum for achieving a good resistance against hot corrosion (e.g. in case of contact with molten glasses [3]). In such case, chromium carbides can be present in microstructure. These carbides are not very stable at high temperatures, and notably less than TaC carbides [4-7] for example. Thus, the knowledge of the volume fractions of chromium carbides at the stable thermodynamic state is important for the prediction of their potential of strengthening on long terms. In addition, the chromium contained in these carbides can be involved in the progress of high temperature oxidation. This phenomenon can induce transformations in the sub-surface microstructure, which can have noticeable consequences for the surface properties of the alloys. Thermodynamic calculations can be very helpful in these two fields: (1) for predicting the volume fraction of chromium carbides available for reinforcing the bulk, and (2) for interpreting the microstructure modifications induced by oxidation in the sub-surface.

In this work, ternary Ni-Cr-C alloys, which can be considered as bases of chromia-forming nickel alloys (30wt.%Cr), with different amounts of carbides (between 0 and 2 wt.%C), were elaborated by casting. Their microstructures after 50 hours of heat treatment were analyzed by metallography. Knowing the nature, volume fractions and

morphologies of the obtained carbides, i.e. their probable strengthening potential, these results about the microstructures of the alloys at almost the thermodynamic stable state can also be used to study the accuracy of a thermodynamic database before its use for an exploration of both a wider range of carbon content and other chromium contents. In a second article, this database will be also used for the characterization of the microstructure transformations in the sub-surface of alloys exposed to oxidation at high temperature.

2. Experimental method

2.1. Synthesis, metallographic preparation and observation

Seven alloys, a binary Ni-30wt.%Cr and six Ni-30wt.%Cr-x%C (residual elements not detectable by microanalysis), with x equal to 0.2, 0.4, 0.8, 1.2, 1.6 and 2wt.%, were cast using pure elements (>99.9%, Alfa Aesar). As always observed for Cr and C for this type of synthesis in previous studies, the chemical compositions of the obtained alloys are very close to the targeted compositions (e.g. Energy Dispersion Spectrometry for Ni and Cr: 30 ± 1 wt.%). Fusion and solidification were performed in a water cooled copper crucible of a high frequency induction furnace (CELES), under an atmosphere of 300mbar of argon gas. The ingots (mass of about 100g in all cases) were cut to {2 × 2 × 8 mm^3}–samples for thermal analysis tests, and {10 × 10 x 3 mm^3}–samples for heat treatments.

The microstructures of the alloys, as cast or after heat treatment, were observed on metallographic samples especially prepared. Initially, each sample was cut in two parts using a precision saw (Buehler Isomet 5000). These parts were firstly embedded in resin (Araldite CY230 + Strengthener Escil HY956). The mounted samples were then polished, first with SiC paper (from 120 to 1,200 grit) under water, and then with 1µm diamond pastes for obtaining a mirror-like surface state. Metallographic observations were done using a XL30 Philips Scanning Electron Microscope (SEM), with the Back Scattered Electrons mode (BSE) and an acceleration voltage of 20 kV. The chemical composition of each alloy was estimated in three locations randomly chosen (total area: 3 × 0.1mm^2), using the Energy Dispersion Spectrometry (EDS) device of the SEM for Ni and Cr. For these elements, the uncertainty was ± 1wt.% for the EDS measurements for all alloys. The carbon contents can be supposed being very close to the targeted ones since this procedure of sample preparation usually leads to a very good respect of the desired carbon contents (verifications were previously done by spark spectrometry for similar alloys).

2.2. Thermal analysis

The solidus and liquidus temperatures were measured by Differential Thermal Analysis (DTA), using a Setaram TG-DTA apparatus, with an alumina crucible under argon. The temperature program applied was: (1) heating at 20 K min^{-1} between room temperature and 1,200 °C, then at 5 K min^{-1} between 1,200 and 1,500 °C, (2) dwell at 1,500°C for about 10 minutes, (3) cooling at -5 K min^{-1} between 1,500 and 1,200 °C, then at -20 K min^{-1} between 1,200 and ambient temperature.

The temperatures corresponding to the starts of fusion and of solidification, and the temperatures corresponding to the ends of fusion and of solidification, were determined. The solidus and liquidus temperatures were supposed to be equal to the values obtained on the heating curve.

2.3. Heat treatments, metallography and thermodynamic calculations

Three samples of each alloy were exposed at three different temperatures, in a high temperature furnace in air. The temperature cycle was (1) heating at 20 K min^{-1} between room temperature and the targeted stage temperature, (2) dwell at high temperature (1,000, 1,100 or 1,200 °C) for 50 hours, and (3) cooling at 10 K min^{-1}.

The samples for metallographic examinations were prepared as described before. The carbides were identified using Wavelength Dispersion Spectrometry (WDS), with a Cameca SX100 microprobe. The same apparatus was also used for measuring the chemical composition in the matrix (in three different locations).

For the determination of the volume fractions of the carbides, micrographs were taken using SEM in the BSE mode, for three locations (areas of about 0.1mm^2) which were randomly selected. The BSE mode, for which the average atomic numbers of the different phases led to different gray levels, allowed an easy separation of matrix (gray) and chromium carbides (dark). The surface fraction of the carbide phase was measured using the Photoshop CS software of Adobe. Each surface fraction was the average value of the measurements performed on the three micrographs, and it was supposed being close to the volume fraction.

For comparison, the carbide volume fractions were determined by an alternate way: by exploiting the differences of chromium content between the matrix (pinpoint WDS measurements) and the whole alloy (global EDS measurements, area of about 0.1mm^2). This was done by calculating the mass fractions of Cr_7C_3 (noted $f_w[Cr_7C_3]$), using equation (1):

$$f_w[Cr_7C_3] = \frac{W_{Cr}[all] - W_{Cr}[mat]}{W_{Cr}[Cr_7C_3] - W_{Cr}[mat]} \quad (1)$$

in which $W_{Cr}[all]$ is the analyzed chromium mass content of the whole alloy, $W_{Cr}[mat]$ the chromium mass content, and $W_{Cr}[Cr_7C_3]$ the theoretical Cr mass content of the Cr_7C_3 carbides ($W_{Cr}[Cr_7C_3]$=0.91). The volume fractions of carbides and of matrix were then calculated according to equation (2):

$$f_v[\phi_j] = \left(\frac{f_w[\phi_j]}{\rho_{\phi j}}\right) / \sum_i \left(\frac{f_w[\phi_i]}{\rho_{\phi i}}\right) \quad (2)$$

in which $f_v[\varphi_j]$, $f_w[\varphi_j]$ and $\rho_{\varphi j}$ are respectively the volume fraction, the weight fraction and the density of the phase φj. The values used for the densities were 8.12 g/cm^3 for matrix (calculated with the measured weights and volumes of the samples) and 6.941 g/cm^3 for the Cr_7C_3 carbides [8].

Calculations were performed for the seven alloys by using the Thermo-Calc software [9] and a database which contains the descriptions of the Ni–Cr–C system and of its sub-systems [10], in order to predict the intervals of fusion/solidification and the microstructures at the three temperatures, for comparison.

3. Results

3.1. The obtained microstructures and comparison with thermodynamic calculations

The as-cast microstructures of the alloys consist of matrix and chromium carbides. Carbides are present with higher fraction when the carbon content is higher. The dendritic structure is not visible in the case of the low carbon Ni02 alloy, but the dendrites of matrix become more obvious for the Ni04, Ni08 and Ni12 alloys. They are not visible again in alloys with very high carbon contents, e.g. in the Ni16 and Ni20 alloys. Indeed, in the latter, carbides are present with high fractions and uniformly dispersed in the microstructure. These microstructures generally are not modified after 50 hours heat treatment (1,000, 1,100 and 1,200°C). One can just notice some coarsening of carbides for 1,200°C. Figure 1 shows the microstructures of all alloys after exposure at 1,000 and 1,200°C, respectively. WDS measurements clearly showed that they are M_7C_3 carbides since the obtained Cr/C atomic ratio was always very close to 2.3. This identification was possible only when the carbides were coarse enough to allow a sufficient accuracy (i.e. for the alloys containing more than 1 wt.%C).

Thermodynamic calculations were performed to know the microstructures predicted from the database for the three temperatures used. The results about natures and mass fractions of the phases existing at 1,000, 1,100 and 1,200°C are presented in Table 1. For all alloys and all temperatures the matrix is always a {face centred cubic}–type solid solution of nickel, and there is only one other phase: the chromium carbide Cr_7C_3, i.e. the same carbide found in the alloys by WDS. For the three temperatures, calculations show that the carbide mass fraction linearly increases when the carbon content increases (i.e. similarly to metallographic observations), and slightly decreases when the holding temperature increases, which was more difficult to see by metallographic observations. For 1,200°C it can be noticed that the calculated Cr_7C_3 mass fraction value could be considered as almost equal to ten times the carbon weight content.

3.2. Chemical composition analyzed in matrix and comparison with calculations

WDS was performed in matrix and led to the values presented in the first of the two lines corresponding to each alloy, in Table 2 (average of three values and standard deviation). Calculations also gave the chromium contents in the matrix and their values are also presented in Table 2. The experimental and calculated chromium contents in the matrix are generally close to each other for almost all alloys and all temperatures.

3.3. Surface fractions of the carbide and comparison with calculations

A first way for the determination of the surface fraction of carbides is image analysis. Such measurements were performed on BSE micrographs using Adobe Photoshop, which led to the surface fractions of carbides presented in Table 3 (average value and standard deviation), in the first one of the two lines for each alloy.

A second way for the determination of the carbide fractions is their deduction from the difference of chromium content between the alloy and its matrix. Indeed, this

allowed assessing the mass fractions of the Cr_7C_3 carbides according to equation (1), then their volume fractions according to equation (2). These surface fractions are also presented in Table 3 (second line for each alloy, first position).

The values of carbide surface fraction belonging to these two sets of experimental measurements were supposed to be close to the corresponding volume fractions. Thus, they can be compared to the carbide volume fractions deduced from the mass fractions calculated by Thermo-Calc, which are also added in Table 3 (second line for each alloy, second position). The three types of carbides volume fractions are consistent and all of them increase when the carbon content increases. The carbide fractions obtained by image analysis and the carbide fractions deduced from the matrix-alloy chromium content differences are generally close to the calculated results.

3.4. Temperature intervals of the mushy state, and comparison with calculations

In order to find temperatures of solidus and liquidus, Differential Thermal Analysis (DTA) was carried out for all alloys. The temperatures of fusion start and of fusion end were considered for the determination of the solidus temperature and of the liquidus temperature, respectively. Figure 2 displays a DTA curve obtained for one of the alloys (Ni08), as illustration. The two endothermic peaks, which correspond to the fusion of the interdendritic {matrix-chromium carbides}-eutectic (first peak) and to the fusion of the matrix (second peak), are clearly visible. The exothermic peaks corresponding to the two solidification sequences can be also clearly seen, in the cooling part of the curve.

The measured solidus and liquidus temperatures are plotted versus the carbon content in the alloy in Figure 3, in which the corresponding values calculated by Thermo-Calc are also added for comparison. The calculated solidus temperatures are consistent with the measured temperatures of fusion start, while this is clearly not the case for the liquidus temperatures. Moreover the difference between the measured temperature of fusion end and the calculated liquidus temperature seems to be increasing with the carbon content.

By comparison with the binary Ni00 alloy, the presence of 0.2 wt.% carbon obviously induces, for the Ni02 alloy, a severe decrease in solidus temperature (measured or calculated). On the contrary, between 0.2 wt.%C and 2.0 wt.%C, the decrease in solidus temperature is very low. The liquidus temperature decreases more regularly, but only until the carbon content reaches about 1.2 wt.%. For carbon contents higher than this value, the measured and calculated liquidus temperatures both increase when the carbon content increases.

4. Discussion

The addition of carbon in a {Ni-30wt.%Cr}–based alloy significantly influences its solidus temperature and the characteristics of its carbides, as previously seen for cobalt alloys also reinforced by chromium carbides [11]. This is of great importance for the aptitude of these nickel alloys to be used as structural materials at high temperature. Thereafter, after having resumed and commented the effects of variations in carbon content on microstructures and on the beginning and end of fusion, one can compare

these experimental results with calculations. This will allow assessing the accuracy of the used database, then its validity to predict microstructures for other compositions. Secondly, this will also allow pointing out the mismatches between measurements and calculations. To finish, the database will be used to explore several other ternary Ni-Cr-C alloys which differ from the ones studied above about the carbon and chromium contents, notably about the types and fractions of carbides.

4.1. Summary of the effects of the enrichment in carbon in a Ni-30wt.%Cr alloy

When the {Ni-30wt.%Cr}–based alloys are enriched in carbon their fraction of carbides becomes increasingly present, as seen by metallography. Above 1.6 wt.% of carbon, the volume fractions of carbides are equal to 20 vol.% or more (which is favorable for hardness and other mechanical properties, but detrimental for ductility and machinability). The dendritic shape of the matrix is more and more visible, because of the more numerous carbides which reveal more and more the interdendritic spaces. Dendrites begin disappearing when the carbon content reaches 1.2%wt.C, and some rare coarse acicular carbides start appearing. These ones are probably the carbides which appeared at the beginning of solidification, before the eutectic solidification.

The refractoriness of the alloys falls when carbon is added to the {Ni-30wt.%Cr}–based alloy. Indeed, the solidus temperature quickly decreases to be equal to the eutectic temperature. For additional fractions of carbon, this eutectic temperature slightly decreases. However it remains above 1,300°C until 1.6wt.%C, which is still sufficiently high to allow applications at high temperature. The liquidus temperature continuously decreases when more and more carbon is added to the Ni-30wt.%Cr base alloy, before the carbon content reaches the eutectic value. It appears that the addition of a little quantity of carbon to the binary Ni-30%wt.Cr alloy, promotes a drastic increase for the temperature interval of solidification. This has usually important consequences on the foundry process since, during the solidification progress, this is favorable for a thick mushy (i.e. solid + liquid) zone along the solidification front, separating the liquid alloy and the fully solidified alloy. Such a thick mushy zone partially obstructs the feeding (by liquid alloy) of the last zone to solidify. It is therefore favorable to the formation of shrinkage defects. However the solidification interval decreases when more carbon is added, down to zero when the eutectic carbon content is reached, which is more favorable for a better metallurgical health of the casting (i.e. lower risk of shrinkage defects or of lacks of feeding by liquid alloy).

4.2. Comparisons between experiments and thermodynamic calculations

The experimental solidus temperatures are in good agreement with the 30%wt.Cr-section of the phase diagram computed with Thermo-Calc (Figure 4). The prediction is excellent about the nature of carbides and, despite some rare exceptions, the Cr-content in the matrix and the volume fractions of carbides are also well predicted by calculations. These good results concerning both carbides and solidus temperatures suggest that this database is efficient to predict levels of refractoriness and stable microstructures (natures and fractions of carbides) with accuracy.

On the contrary there is a significant mismatch between the experimental liquidus temperatures and the calculated ones, and this difference becomes greater for higher carbon contents. There is also a shift of the eutectic carbon content between calculations (about 1.5%wt.C) and experiments (about 1.2%wt.C). It is possible that the database is not as efficient for calculating the liquidus as for predicting the solidus and the natures and fractions of carbides. But one can think that the efficiency of the DTA measurements is probably lower for the end of fusion than for the start of fusion. Indeed, firstly the measured liquidus temperature remains significantly higher than the solidus temperatures at the apparent eutectic carbon content (about 1.2wt.%C according to DTA) and secondly this eutectic carbon content is significantly lower than the calculated one: about 1.5wt.%C which is moreover confirmed by the microstructure transition between Ni12 (containing dendrites of matrix) and Ni16 (no dendrite).

4.3 Microstructure evolutions of carbon-containing Ni-base alloys for varying chromium contents

Table 4 presents the results obtained by calculations for alloys with varying chromium contents around 30 mass.%Cr and for three carbon contents from 0 to 2 wt.% at 1,100°C. The microstructure generally contains M_7C_3 carbides with mass fractions (or volume fractions) which vary with the carbon content. The chromium content has also an influence on the carbide fractions, but it is more limited. In addition one can see that the carbide stoichiometry can change when the carbon content or the chromium content is modified. When the Cr content is low (20–25 wt.%) and the C content is high (2 wt.%), the stable carbide is Cr_3C_2, instead of M_7C_3. When the Cr content is high (30–35 wt.%) and the C content is not very high, the stable carbide is $M_{23}C_6$. Graphite can appear when the atomic ratio Cr/C becomes particularly low. The type of matrix remains similar for all compositions.

Thus it can be useful to know that a change of the chromium content (in order to increase the resistance of the alloy against high temperature corrosion) or of the carbon content (in order to increase its strength or its hardness) may lead to other carbide formation. Some of these microstructural changes can sometimes play a detrimental role for properties. For instance, graphite may affect the resistance against high temperature oxidation, as well as the toughness and the strength of the alloys.

4.4 Microstructure evolutions of {30 wt.% Cr}–containing Ni-base alloys for carbon contents higher than 2 wt.%

When the carbon content is increased to values above 2 wt.%, the microstructure of the alloy can be significantly modified. Table 5 presents some examples of three high carbon contents for the 20–40 wt.%Cr range. For the chromium contents which are usually encountered with nickel alloys for high temperature applications (20–30 wt.%Cr.), the three considered carbon contents lead to the presence of the carbon-richest carbides (Cr_3C_2) and also of graphite. The M_7C_3 carbide phase appears only when the chromium content is particularly high (40 wt.%Cr), and it is the sole type of carbide only if the carbon content is 3 wt.%. For the two higher values of the carbon content, the M_3C_2 also exists and can become the main carbide phase for 5 %wt.C. For

avoiding the presence of graphite, the chromium content must be very high when the carbon content is higher than 3 wt.%.

4.5 Microstructure evolutions of {30 wt.%Cr}–containing Ni-base alloys for very low carbon contents

On the contrary, when one considers the very low carbon contents, it appears that there are Ni-Cr-C alloys which can contain carbon but no carbides at high temperatures. However their carbon contents are necessarily very low. Table 6 shows the maximal values of carbon content allowing the absence of carbides at different high temperatures and for three chromium contents, i.e. the carbon content corresponding to the solvus. For a given chromium content the solvus carbon content increases with temperature, while, for a given temperature, the solvus carbon content decreases when the chromium content increases. Thus, when carbides are not desired in a nickel-chromium alloy, the quantity of carbon (present as impurities for example) must be very low. This is especially true for low temperatures and for high chromium contents. Another field in which a local absence of carbides can be encountered is the high temperature oxidation of carbides-strengthened nickel-chromium alloys. Indeed, in such situation, a zone without carbides develops from the external surface and thermodynamic calculations can show that almost the whole carbon which was initially present here, necessarily left this growing zone in which carbides were disappearing because of oxidation.

6. Conclusions

The experimental and metallographic results of this study concerning Ni-{30wt.%Cr-0 to 2wt.%C}-type alloys show a complete description of their microstructures at high temperature. Different degrees of strengthening by carbides can be obtained without significant loss of refractoriness, while different morphologies of the carbides (all Cr_7C_3) were observed (depending more on the carbon content than on temperature). Their measured volume fraction increases with the carbon content, and they can be found again by thermodynamic calculations. The thermodynamic tool used here is very accurate for predictions about microstructure (nature and fractions of carbides) and refractoriness (solidus temperatures). This efficient prediction of the solid states at high temperature is the main requirement for the use which will be done in the second part of this study [12]. Indeed this one will deal with the solid-state phenomena which sometimes occur in the sub-surface of alloys of this type, when they are subjected to high temperature oxidation.

Acknowledgements

The authors thank the Microanalysis Common Service of the Faculty of Sciences and Techniques of Nancy, especially Sandrine Mathieu and Johann Ravaux.

References

[1] E. F. Bradley, Superalloys: A Technical Guide, ASM International, 1988.
[2] C. T. Sims, W. C. Hagel, The Superalloys, John Wiley & Sons, 1972.
[3] P. Kofstad, *High Temperature Corrosion*, Elsevier applied science, 1988.
[4] P. Berthod, S. Michon, L. Aranda, S. Mathieu, J.C. Gachon, Calphad 27 (2003) 353-359.
[5] P. Berthod, L. Aranda, C. Vébert, S. Michon, Calphad 28 (2004) 159-166.
[6] P. Berthod, Y. Hamini, L. Aranda, L. Héricher, Calphad 31 (2007) 351-360.
[7] P. Berthod, Y. Hamini, L. Héricher, L. Aranda, Calphad 31 (2007) 361-369.
[8] Handbook of Chemistry and Physics, 57th edition (1976-1977).
[9] Thermo-Calc version N: "Foundation for Computational Thermodynamics" Stockholm, Sweden, Copyright (1993, 2000). www.thermocalc.com
[10] SGTE: “Scientific Group Thermodata Europe” database, update 1992, http://www.SGTE.org.
[11] P. Berthod, P. Lemoine, J. Ravaux, Journal of Alloys and Compounds, in press (doi:10.1016/j.jallcom.2007.12.023).
[12] P. Berthod, submitted to Calphad.

TABLES

Table 1
Mass fractions of carbides at 1,000, 1,100 and 1,200°C according to Thermo-Calc calculations (matrix is of the {face centred cubic}–type for all alloys at all temperatures)

Calculated microstructure	1,000°C	1,100°C	1,200°C
Ni20	M_7C_3 (21.33 wt.%)	M_7C_3 (21.01 wt.%)	M_7C_3 (20.67 wt.%)
Ni16	M_7C_3 (17.26 wt.%)	M_7C_3 (17.01 wt.%)	M_7C_3 (16.72 wt.%)
Ni12	M_7C_3 (13.01 wt.%)	M_7C_3 (12.82 wt.%)	M_7C_3 (12.58 wt.%)
Ni08	M_7C_3 (8.66 wt.%)	M_7C_3 (8.51 wt.%)	M_7C_3 (8.32 wt.%)
Ni04	M_7C_3 (4.26 wt.%)	M_7C_3 (4.15 wt.%)	M_7C_3 (3.99 wt.%)
Ni02	M_7C_3 (2.06 wt.%)	M_7C_3 (1.95 wt.%)	M_7C_3 (1.81 wt.%)

Table 2
Chromium contents in the matrix at 1,000°C, 1,100°C and 1,200°C, measured by WDS (three measurements; calculation of the average value and of the standard deviation); comparison with values issued from Thermo-Calc calculations

Meas. Cr (wt.%)	± σ	1,000°C		1,100°C		1,200°C	
Calculated Cr (wt.%)							
Ni20	Measured	14.35	± 0.15	15.56	± 0.33	18.81	± 0.89
	Calculated	14.88		15.62		16.39	
Ni16	Measured	17.91	± 0.06	18.24	± 0.07	18.42	± 0.26
	Calculated	17.96		18.45		19.00	
Ni12	Measured	21.46	± 0	21.71	± 0.04	21.71	± 0.23
	Calculated	21.20		21.50		21.86	
Ni08	Measured	22.46	± 0.31	23.03	± 0.09	23.35	± 0.15
	Calculated	24.36		24.54		24.76	
Ni04	Measured	26.97	± 0.28	27.21	± 0.04	27.24	± 0.13
	Calculated	27.33		27.44		27.57	
Ni02	Measured	29.50	± 0.16	28.50	± 0.11	28.73	± 0.24
	Calculated	28.74		28.82		28.92	

Table 3
Experimental volume fractions of carbides, either deduced from the weight contents of chromium measured in the matrix, or directly measured by image analysis (average value ± 1 standard deviation); comparison with values issued from Thermo-Calc calculations

Exp f_{vol} Surf Anal (%) / Exp f_{vol} Calc %Cr (%)	± σ (%) / Cal. f_{vol} (%)	**1,000°C**		**1,100°C**		**1,200°C**	
Ni20		26.07	± 1.42	21.88	± 1.84	23.31	± 1.25
		23.09	24.08	21.69	23.73	17.67	23.36
Ni16		20.73	± 1.00	19.76	± 0.80	20.03	± 1.30
		18.83	19.62	18.40	19.34	18.17	19.02
Ni12		14.48	± 0.78	17.55	± 0.45	15.60	± 1.60
		14.07	14.89	13.71	14.68	13.71	14.41
Ni08		11.60	± 0.14	10.30	± 0.44	9.12	± 0.54
		12.64	9.98	11.79	9.81	11.31	9.60
Ni04		3.05	± 0.75	4.54	± 0.93	5.58	± 0.22
		5.49	4.95	5.08	4.82	5.02	4.64
Ni02		1.25	± 0.08	1.93	± 0.19	2.12	± 0.06
		1.01	2.40	2.80	2.27	2.39	2.11

Table 4
Carbide formations at 1,100°C with Cr variations, according to Thermo-Calc calculations (matrix is of the {face centred cubic}–type for all alloys)

Computed µstructure	0.5 wt.%C	1 wt.%C	2 wt.%C
40 wt.%Cr	$M_{23}C_6$ (8.66 wt.%)	M_7C_3 (3.60 wt.%) + $M_{23}C_6$ (11.72 wt.%)	M_7C_3 (21.97 wt.%)
35 wt.%Cr	M_7C_3 (4.24 wt.%) + $M_{23}C_6$ (1.77 wt.%)	M_7C_3 (10.86 wt.%)	M_7C_3 (21.71 wt.%)
30 wt.%Cr	M_7C_3 (5.24 wt.%)	M_7C_3 (10.67 wt.%)	M_7C_3 (21.01 wt.%)
25 wt.%Cr	M_7C_3 (4.98 wt.%)	M_7C_3 (10.18 wt.%)	M_3C_2 (6.37 wt.%) + M_7C_3 (10.47 wt.%)
20 wt.%Cr	M_7C_3 (4.33 wt.%)	M_7C_3 (8.93 wt.%)	Graphite (3×10^{-28} wt.%) + M_3C_2 (12.31 wt.%)

Table 5
Carbides existing at 1,100°C when the carbon content increases to higher values than the 2 wt.%C of the Ni20 alloy, according to Thermo-Calc calculations (matrix is of the {face centred cubic}–type for all alloys)

Computed microstructure	20 wt.%Cr	30 wt.%Cr	40 wt.%Cr
5.0 wt.%C	Graphite (2.82 wt.%) + M_3C_2 (13.38 wt.%)	Graphite (1.16 wt.%) + M_3C_2 (26.22 wt.%)	M_3C_2 (35.68 wt.%) + M_7C_3 (0.82 wt.%)
4.0 wt.%C	Graphite (1.83 wt.%) + M_3C_2 (13.25 wt.%)	Graphite (0.17 wt.%) + M_3C_2 (26.09 wt.%)	M_3C_2 (8.48 wt.%) + M_7C_3 (30.42 wt.%)
3.0 wt.%C	Graphite (0.84 wt.%) + M_3C_2 (13.12 wt.%)	M_3C_2 (16.14 wt.%) + M_7C_3 (7.25 wt.%)	M_7C_3 (32.72 wt.%)

Table 6
Solvus carbon contents for different chromium contents and different high temperatures (values determined by thermodynamic calculations)

Maximal possible C content (wt.%)	1,000°C	1,100°C	1,200°C
40 wt.%Cr	0.004	0.008	0.015
30 wt.%Cr	0.013	0.023	0.035
20 wt.%Cr	0.0434	0.071	0.108

FIGURES

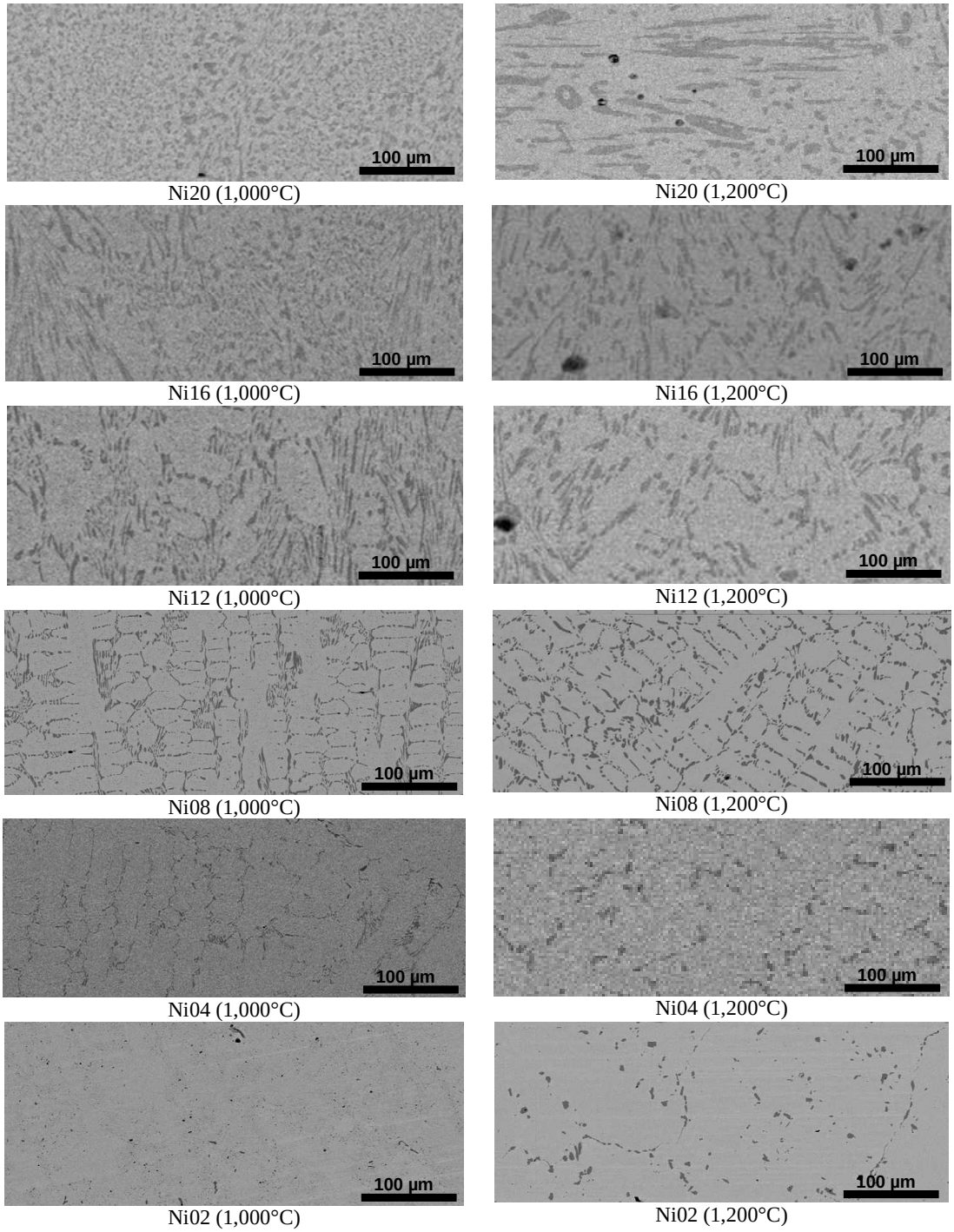

Fig. 1. Microstructures of all alloys heat treated for 50 hours at 1,000 and 1,200°C respectively (pictures taken with SEM in BSE mode).

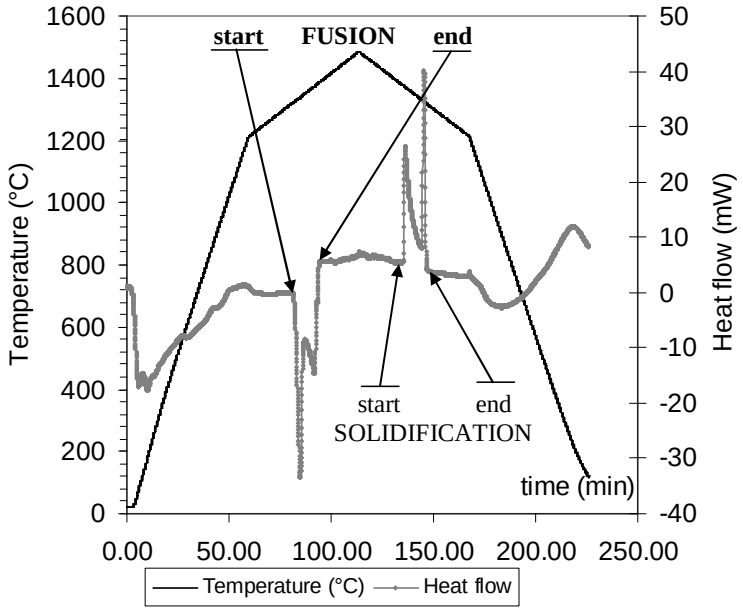

Fig. 2. Example of a DTA curve with determination of the temperatures of the **start and end of fusion (values considered in this study)** and of start and end of solidification (here: case of the Ni08 alloy).

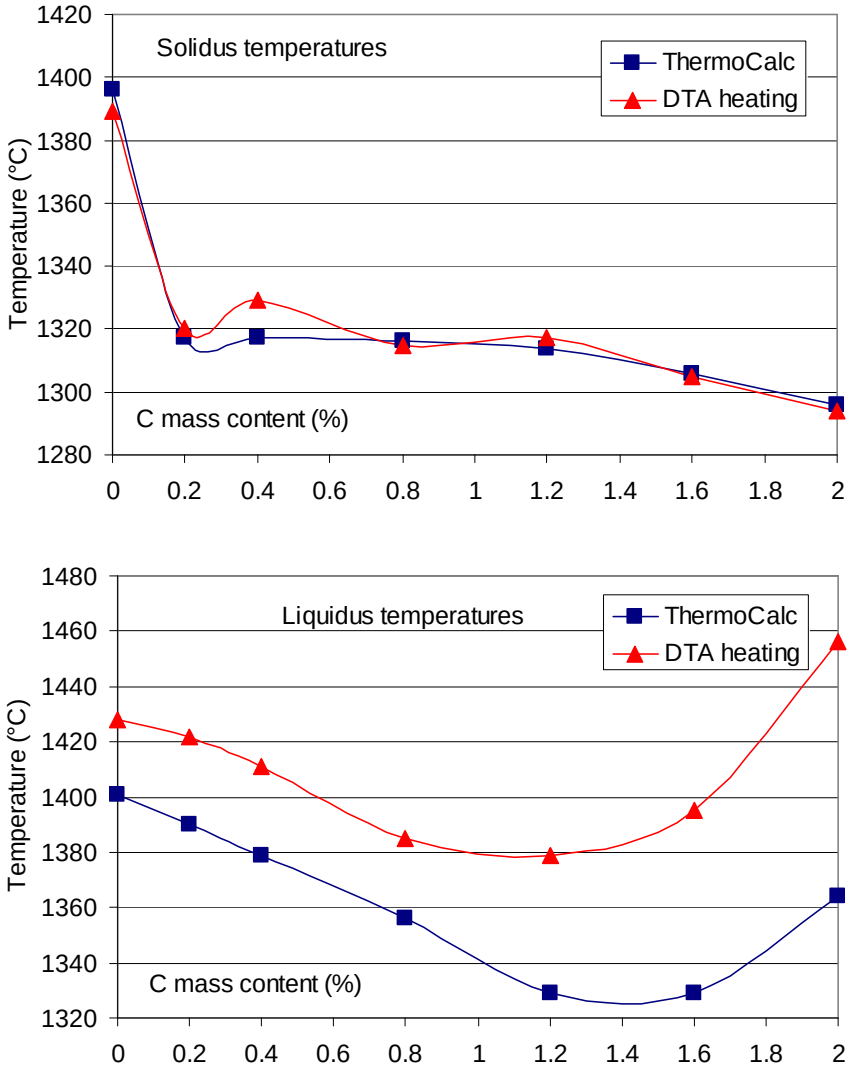

Fig. 3. The solidus and liquidus temperatures plotted versus the carbon content: calculated (Thermo-Calc) and measured (DTA curves; determination on their heating part).

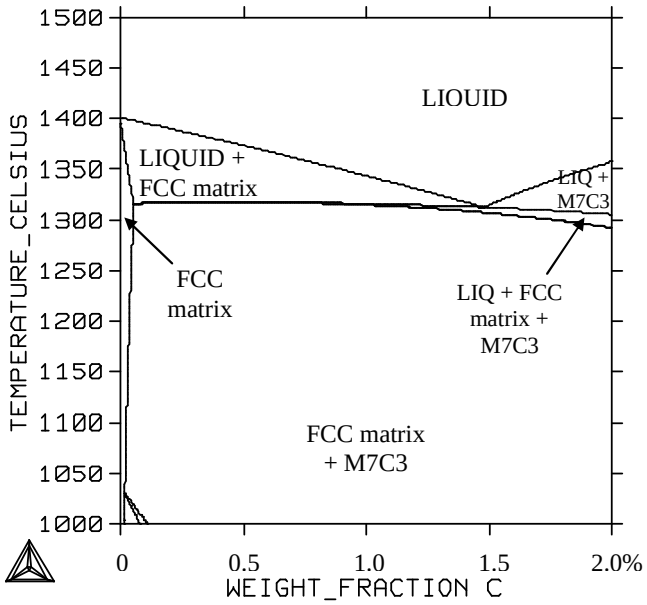

Fig. 4. Section at 30 wt.%Cr of the Ni-Cr-C diagram issued from Thermo-Calc calculations.